

UCLA

UCLA Previously Published Works

Title

Pushing the limits of detectability: mixed dark matter from strong gravitational lenses

Permalink

<https://escholarship.org/uc/item/5648q967>

Journal

Monthly Notices of the Royal Astronomical Society, 524(4)

ISSN

0035-8711

Authors

Keeley, Ryan E

Nierenberg, Anna M

Gilman, Daniel

et al.

Publication Date




2023-07-29

DOI

10.1093/mnras/stad2251

Peer reviewed

Pushing the limits of detectability: mixed dark matter from strong gravitational lenses

Ryan E. Keeley ¹★, Anna M. Nierenberg,¹ Daniel Gilman,² Simon Birrer,^{3,4} Andrew Benson ⁵ and Tommaso Treu ⁶

¹*Department of Physics, University of California Merced, 5200 North Lake Road, Merced, CA 95343, USA*

²*Department of Astronomy and Astrophysics, University of Toronto, Toronto, ON M5S 3H4, Canada*

³*Department of Physics, Kavli Institute for Particle Astrophysics and Cosmology, Stanford University, Stanford, CA 94305, USA*

⁴*SLAC National Accelerator Laboratory, Menlo Park, CA 94025, USA*

⁵*Carnegie Institution for Science, 813 Santa Barbara Street, Pasadena, CA 91101, USA*

⁶*Department of Physics and Astronomy, University of California, Los Angeles, CA 90095, USA*

Accepted 2023 July 19. Received 2023 July 19; in original form 2023 February 2

ABSTRACT

One of the frontiers for advancing what is known about dark matter lies in using strong gravitational lenses to characterize the population of the smallest dark matter haloes. There is a large volume of information in strong gravitational lens images – the question we seek to answer is to what extent we can refine this information. To this end, we forecast the detectability of a mixed warm and cold dark matter scenario using the anomalous flux ratio method from strong gravitational lensed images. The halo mass function of the mixed dark matter scenario is suppressed relative to cold dark matter but still predicts numerous low-mass dark matter haloes relative to warm dark matter. Since the strong lensing signal receives a contribution from a range of dark matter halo masses and since the signal is sensitive to the specific configuration of dark matter haloes, not just the halo mass function, degeneracies between different forms of suppression in the halo mass function, relative to cold dark matter, can arise. We find that, with a set of lenses with different configurations of the main deflector and hence different sensitivities to different mass ranges of the halo mass function, the different forms of suppression of the halo mass function between the warm dark matter model and the mixed dark matter model can be distinguished with 40 lenses with Bayesian odds of 30:1.

Key words: gravitational lensing: strong – methods: statistical – galaxies: structure – dark matter.

1 INTRODUCTION

Λ CDM, Λ for a cosmological constant type dark energy, and CDM for cold dark matter (DM), has maintained its status as the standard model (SM) of cosmology over the past generation of cosmological observations. With just a few parameters, it can explain most of the Universe. The broader goal of much of cosmology is to identify the nature of these components of Λ CDM, in particular for astroparticle physics, the nature of DM. One strategy to identify the nature of DM is to look for any SM DM annihilation products (indirect detection; Gaskins 2016), collisions of DM with SM particles (direct detection; Schumann 2019), or to produce DM from SM particles at colliders (Kahlhoefer 2017).

Examples of specific DM models include the weakly interacting massive particles (WIMPs) and sterile neutrinos, with all of their various production mechanisms (Dodelson & Widrow 1994; Shi & Fuller 1999; Abazajian, Fuller & Patel 2001; Kusenko 2009; Abazajian 2017; Abazajian & Kusenko 2019). However, the simplest indirect detection of WIMP annihilation from the largest, closest DM source to Earth, the Galactic Centre, is ruled out (Abazajian et al. 2020). Thus, it is prudent to look at other probes for hints of DM's

particle nature, though measuring the distribution of DM (e.g. halo mass function) is interesting regardless of any results from indirect detection.

For instance, rather than probing DM's interactions with the SM, one can probe DM's phenomenological properties (i.e. whether there is a suppression in the amount of clustering relative to CDM, or whether DM interacts with itself) via its gravitational interactions. The CDM paradigm, which posits DM is collisionless as well as cold, predicts the existence of collapsed DM haloes down to very small halo masses (equivalently very short length scales; Metcalf & Madau 2001; Dutton & Macciò 2014; Despali et al. 2016; Angulo et al. 2017). Thus, measuring the distribution of DM on small scales can serve as a useful determination of DM phenomenology and can serve as a hint towards identifying the particle nature of DM. Importantly, the distribution of DM throughout the Universe can be probed by only characterizing its gravitational interactions, such as with strong gravitational lensing (Mao & Schneider 1998; Metcalf & Madau 2001; Dalal & Kochanek 2002; Chen, Kravtsov & Keeton 2003; Moustakas & Metcalf 2003; Metcalf 2005; Amara et al. 2006; Miranda & Maccio 2007; Minezaki et al. 2009).

The missing satellite problem is motivation for thinking that warm DM (WDM) might more accurately describe the Universe than CDM (Viel et al. 2013). The smallest DM haloes, that Λ CDM predicts in abundance, were not observed in the Local Group or

* E-mail: rkeeley@ucmerced.edu

cosmologically, such that it was once thought to be a possibility that the halo mass function was suppressed on the dwarf scale (Nierenberg et al. 2016; Robles, Bullock & Boylan-Kolchin 2019). However, the most recent generations of telescopes have detected populations of ultrafaint dwarf galaxies, which have, for certain assumptions about star formation and completeness corrections, constrained deviations between WDM and CDM subhalo mass functions to be only on subgalactic scales. Further, some simulations, along with specific assumptions about star formation, baryonic feedback, and tidal stripping, show that subhaloes are destroyed more efficiently than originally thought from DM only simulations (Kim, Peter & Hargis 2018; Kim & Peter 2021).

Beyond either the CDM or WDM paradigms, the cosmological DM could be composed of multiple particles with different phenomenological properties (Boyersky et al. 2009; Anderhalden et al. 2012; Kamada, Inoue & Takahashi 2016; Paribelli et al. 2021; Vogt, Marsh & Laguë 2022). Specifically, we investigate a case where half of the DM is composed of CDM particles and half is WDM particles. We refer to this case as mixed DM (MixDM). There are a wide variety of plausible scenarios in which MixDM could be realized. For instance, many models have three generations of sterile neutrinos with different masses from keV to GeV (Kusenko 2009; Patwardhan et al. 2015; Abazajian 2017). With different masses and potentially different resonances in their production mechanism, such multiple generations of sterile neutrinos could have a complicated transfer function compared to CDM (Abazajian & Kusenko 2019; Vogel & Abazajian 2022). Another possibility is that WIMPs could play the role of CDM and axions could play the role of fuzzy DM (as the component that has less power on small scales; Niemeyer 2020). We are not trying to make the case that MixDM should be a priori expected, but to present a not-unreasonable model that offers a test for what should be detectable with upcoming observations of strong lens systems with *JWST*.

In strong gravitational lensing, the light from a source is deflected by the combined gravitational potential of a main deflector lens and all of the subhaloes and line-of-sight haloes along the trajectory the light follows to create multiple images of the source. In certain configurations of the lens, four distinct images will be created. Analysing the fluxes of these images can allow us to make inferences about the mass function of low mass DM haloes (Mao & Schneider 1998; Metcalf & Madau 2001; Dalal & Kochanek 2002; Chen et al. 2003; Moustakas & Metcalf 2003; Metcalf 2005; Amara et al. 2006; Miranda & Maccio 2007; Minezaki et al. 2009; Gilman et al. 2017, 2018, 2020b; Laroche et al. 2022).

Further, since strong gravitational lensing can probe completely dark haloes, it can probe the physics of the least massive haloes at the smallest scales, both in the lens and along the line of sight, which is where deviations from CDM are expected to be found. Because they are dark, any potential signal of DM physics would not be confused for new baryonic/stellar physics. Low-mass DM haloes are hard to probe since they are not efficient at forming galaxies. However, these low-mass DM haloes can be ‘seen’ via their gravitational interactions, such as in strong gravitational lensing of quasars by galaxies. New DM physics from WDM, self-interacting DM (SIDM), collisional, and fuzzy DM predict novel configurations and distributions of low-mass DM haloes that could explain the small-scale structure of DM haloes. Thus, characterizing the distribution and profiles of these lowest mass DM haloes with strong gravitational lenses could provide evidence for novel DM physics.

Strong lens systems can be used not just to infer the abundance of DM haloes but also their concentrations (Gilman et al. 2020b). Indeed, recent works have found subhaloes that have a concentration

much higher than would be expected in Λ CDM and may point towards SIDM (Andrade et al. 2019, 2021; Minor et al. 2021a, b; Gilman, Zhong & Bovy 2022).

There are two techniques that are commonly employed that use strong gravitational lenses to infer the properties of DM: the flux ratio anomaly method and gravitational imaging. The key difference between these methods is the size of the source observed. The flux ratio anomaly method, which we employ in this work, uses sources of sufficiently small size, such that the lens will create four distinct point sources (Dalal & Kochanek 2002; Gilman et al. 2019, 2020b, 2021, 2022; Hsueh et al. 2020). In contrast, gravitational imaging uses larger sources, such that the lens will create extended arcs (Vegetti et al. 2018; Enzi et al. 2021). The idea with the flux ratio anomaly method is to examine perturbations in the fluxes of quadruply imaged quasars, relative to the predictions of the main deflector. The anomalous flux ratio method works by using the image positions to constrain the smooth mass distribution of the main deflector lens and predict values for the observed flux ratios. Any additional perturbations from subhaloes and line-of-sight haloes will affect the flux ratios. These perturbations amount to detections of a population of DM haloes and the modelling of these perturbations, in a statistical sense, can yield information about the statistical properties of the population of DM haloes, and thus the physics that generated them. Existing constraints using this method place the mass of a thermally produced WDM relic at $m_{\text{WDM}} > 9.7$ keV (Nadler et al. 2021). There is a lot of information in this quad lens system and so we seek to understand how far we can refine that information.

In this paper, we investigate the potential for strong lens systems, as measured by upcoming *JWST* observations, to detect novel DM physics beyond either the CDM and WDM paradigms, e.g. a MixDM model. We elaborate on the details of this model in Section 2. We further discuss the details of the flux ratio anomaly method from strong lens systems in Section 3 and the details of our statistical methods in Section 4. We present the results of our forecasts in Section 5 and conclude in Section 6.

2 MIXED DARK MATTER

One way to extend the CDM paradigm is to allow the DM particle to be slightly warm. This WDM particle would free stream a non-negligible distance over the age of the Universe and the WDM particle would therefore diffuse out of small overdensities in the matter field and delay the collapse and growth of DM haloes. Any amount of free streaming of particle DM can wash out structure on scales below the free-streaming length (Bond et al. 1983; Green et al. 2004). Lighter particles free stream for longer times and thus will wipe out more structure. For thermally produced relics, WDM composes a subclass of sub-GeV DM candidates. It is this special case for which constraints on a WDM mass are often quoted, but the power of arguments based on structure formation allows one to recast an inference of the free-streaming length in the context of any DM model with a cosmologically relevant free-streaming length, such as sterile neutrinos (Zelko et al. 2022).

Examples of a WDM candidate include sterile neutrinos, axions, gravitinos, or any light thermally produced relic (Colombi et al. 1996; Abazajian 2017; Vogel & Abazajian 2022). The microphysics of specific WDM models can influence greatly the mapping between particle properties, such as the mass, and astrophysical observables, such as the power spectrum (Abazajian 2017; Vogel & Abazajian 2022). Typically, however, when lower limits on DM masses are quoted, it is assumed that the WDM particle followed a thermal

distribution at early times. This is important to keep in mind, since if, for example, a sterile neutrino was resonantly produced with lower momentum, compared to a generic thermal relic of the same mass, then it would appear colder (Abazajian 2017). Such a model could include a ‘chilly’ sterile neutrino. Thus, certain models of sterile neutrino production can evade existing bounds on the WDM mass yet still explain potential signals like the 3.55 keV line which would be explained by the decay of a 7.1 keV sterile neutrino (Abazajian 2017).

Similarly, the half-mode mass (M_{hm}), the mass of the DM halo that corresponds to a decrease in the WDM transfer function by a factor of one-half relative to the CDM transfer function, is a useful parameter that summarizes the suppression of structure at small scales. This is a characteristic scale at which a suppression in small-scale structure should become observable. We can probe half-mode masses down to $10^{6.5} M_{\odot}$ with strong lensing observed with the *JWST*. In an upcoming *JWST* programme (GO-2046; PI Nierenberg), we will measure flux ratios with ~ 3 per cent relative precision, which, based on the forecasting of Gilman et al. (2019), will enable us to either rule out or detect half-mode masses above $10^7 M_{\odot}$.

Of course, there is no a priori reason for the dark sector to be simple, no reason for DM to be a single entity. Indeed, the totality of the cosmological DM could be composed of all of the well-motivated WDM candidates, sterile neutrinos, axions, gravitinos, etc. Being composed of different kinds of particles, such a MixDM could have different clustering properties. So, we are interested in to what extent we can constrain such a complicated DM scenario with the large set of future strong gravitational lenses we will observe with *JWST*. Specifically for this paper, we are investigating a MixDM case, where 50 per cent of the DM is cold and 50 per cent is warm.

We first implement the MixDM model using the cosmological software CLASS (Lesgourgues 2011), which we use to calculate the transfer function for our model. The cosmology for these calculations was taken to be the Planck 2018 best-fitting cosmology (Planck Collaboration VI 2020). We take the best-fitting density of CDM and then take half of that density and assign it to a WDM component. We then calculate a halo mass function resulting from this transfer function using GALACTICUS (Benson 2012) with the Sheth–Tormen (Sheth & Tormen 1999) halo mass function.

Since the software we use to populate our lens models with DM haloes, PYHALO, which renders full mass distributions for substructure lensing simulations with the open source gravitational lensing software package LENSTRONOMY, requires a parametrized form of the halo mass function, we fit the output halo mass function from CLASS (Lesgourgues 2011) and GALACTICUS (Benson 2012) as a suppression relative to the CDM mass function:

$$\frac{dN/dM_{\text{MixDM}}}{dN/dM_{\text{CDM}}}(M) = \left(f + (1-f) \left(1 + a \left(M_{\text{hm}}/M \right)^b \right)^{c/2} \right)^2, \quad (1)$$

where, a , b , and c are parameters describing the WDM suppression relative to CDM and we fix them to $a = 0.5$, $b = 0.8$, and $c = -3.0$. Also, f is the fraction of CDM, which we set to 0.5 in our analyses.

Intuitively, the f^2 in the mass function comes from the fact that there is an f^2 factor in the suppression in the power spectrum, since the power spectrum is a two-point statistic. Consider,

$$\begin{aligned} \rho_{\text{DM}} &= f \rho_{\text{CDM}} + (1-f) \rho_{\text{WDM}} \\ \langle \rho_{\text{DM}} \rho_{\text{DM}} \rangle &= f^2 \langle \rho_{\text{CDM}} \rho_{\text{CDM}} \rangle \\ &+ f(1-f) \langle \rho_{\text{CDM}} \rho_{\text{WDM}} \rangle + (1-f)^2 \langle \rho_{\text{WDM}} \rho_{\text{WDM}} \rangle. \end{aligned}$$

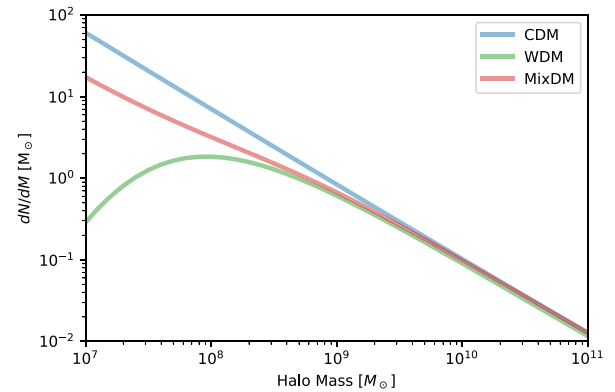


Figure 1. Example halo mass functions for CDM (blue), WDM (green), and MixDM (red) cases, where the warm component of the MixDM case has the same mass as the WDM case, specifically, that the $M_{\text{hm}} = 10^{8.5} M_{\odot}$ for both models.

At sufficiently small scales, only the $f^2 \langle \rho_{\text{CDM}} \rho_{\text{CDM}} \rangle$ term remains. Ultimately, this intuition is verified by our GALACTICUS calculations.

Further, the concentration–mass relation for MixDM is set to be identical to the WDM one which we use from Bose et al. (2016). This is a conservative choice when trying to differentiate MixDM and WDM. One would need to simulate a MixDM universe in order to robustly calculate the concentration–mass relation for this MixDM model.

In Fig. 1, we plot a MixDM case, WDM case, and CDM case assuming the Planck 2018 best-fitting cosmology (Planck Collaboration VI 2020). As we see in Fig. 1, the MixDM case is suppressed relative to CDM, but there is no turnover and the lowest mass haloes are still abundant compared to the WDM case. Since the strong lensing signal receives a contribution from a range of DM halo masses, the signal is less sensitive to the specific features of any model’s halo mass function, but instead is sensitive to the total amount of suppression (see Section 3). So, we are investigating to what extent would WDM or MixDM scenarios be confused for one another.

3 STRONG LENSING DETAILS

Strong gravitational lenses are an exciting probe of DM physics as they can probe the mass function and structure of haloes at cosmological distances regardless of whether they host galaxies. In a strong lens system, the positions and magnifications of the multiple images depend on the first and second derivatives of the gravitational potential, respectively. The image positions typically offer a robust constraint on the model of the main deflector (Gilman et al. 2017, 2018). The second derivative of the lens’ gravitational potential is greatly altered by the presence of low-mass haloes and thus the fluxes of the images are sensitive to them. The magnification field can be calculated at any point on the sky. Since the sources have finite sizes, the actual magnification of the images is integrated over a finite region of the sky. Typically, smaller source sizes are sensitive to smaller halo masses since the effect of perturbations is integrated over the size of the source in the image plane.

As mentioned previously, we employ the flux ratio anomaly method in quadruply lensed images. Since the model of the main deflector gives a range of predictions for the fluxes of the four images, any additional DM haloes that are satellites of the main deflector (subhaloes) or haloes along the line of sight would perturb the predictions of the four images’ fluxes. So, this anomalous flux

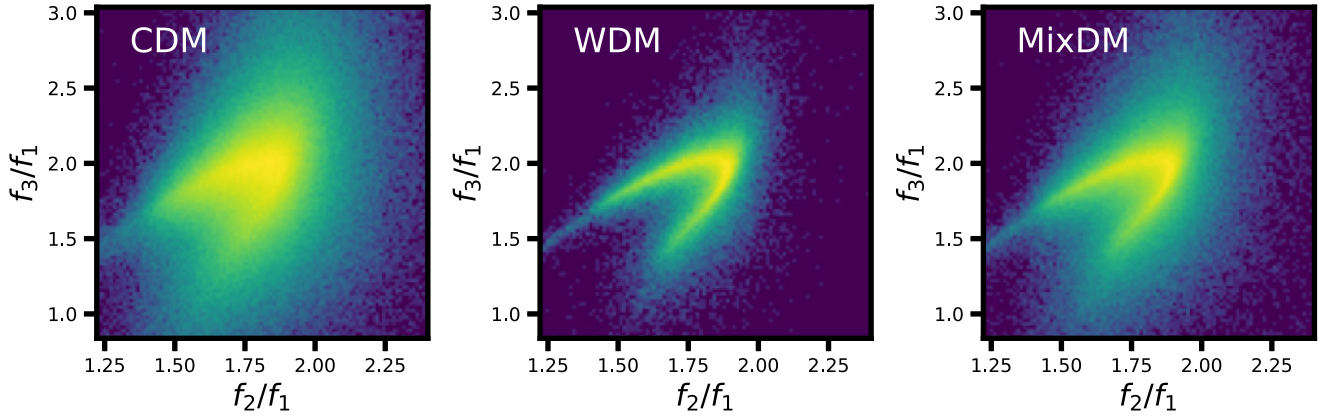


Figure 2. Example 2D histograms of flux ratios (f_i are the flux ratios of individual images) for CDM, WDM, and MixDM cases. The width of the distributions corresponds to the statistical signal that we seek to use to differentiate these models.

is the statistical signal that would give information about the halo mass function, the DM’s transfer function, and ultimately about the particle identity of DM.

Narrow line emission from quasars has been the main source of data in the past (Nierenberg et al. 2020) and this will continue to improve as larger data sets at higher resolution and precision are acquired with improved adaptive optics and instruments such as Keck All-sky Precision Adaptive-optics (KAPA) (Wizinowich et al. 2022) and LIGER (Wright et al. 2019) currently under development at Keck. Furthermore, the launch of *JWST* has opened up the new exciting possibility to use flux ratios measured in the mid-infrared, where the source is typically smaller than the narrow line emission and thus more sensitive to low-mass perturbations. The cold torus regions of quasars, detectable by *JWST*-MIRI, typically have source sizes in the range 1–10 pc, which is small enough to be sensitive to individual $10^7 M_\odot$ haloes. Thus, when we make our mock lensed images, we take a source size of 5 pc.

Even in CDM, the processes by which subhaloes and the satellite galaxies that inhabit them infall into and evolve within the host DM halo are very dynamical and non-linear and thus uncertain. Currently, we marginalize over this uncertainty with a parameter describing the normalization of the subhalo mass function, Σ_{sub} , which is defined, following Gilman et al. (2020a), such that,

$$\frac{d^2N}{dM dA} = \frac{\Sigma_{\text{sub}}}{M_0} \left(\frac{M}{M_0} \right)^\alpha \mathcal{F}(M_{\text{halo}}, z), \quad (2)$$

where α is the slope of the subhalo mass function, the pivot halo mass is fixed to $M_0 = 10^8 M_\odot$, and $\mathcal{F}(M_{\text{halo}}, z)$ is a function that encapsulates the dependence of the subhalo mass function on host halo mass and redshift and is calibrated on results from GALACTICUS. This parameter introduces large degeneracies in the inference of DM properties.

We model these strong lens systems with LENSTRONOMY (Birrer & Amara 2018; Birrer et al. 2021). Using the halo mass functions calculated with GALACTICUS, we implement the MixDM model in PYHALO.

We generate 40 mock lenses from the MixDM model using a variety of main deflector configurations with different realizations of line-of-sight haloes. Subhalo populations were drawn from the MixDM model using parameters $M_{\text{hm}} = 10^{8.5} M_\odot$ and $\Sigma_{\text{sub}} = 0.05 \text{ kpc}^{-2}$.

4 CHARACTERIZING THE MIXDM SIGNAL

We perform an initial test to determine whether the signals from the three DM models can be distinguished statistically. Specifying the parameters of a DM model’s halo mass function does not specify a single set of flux ratios, but instead a distribution of flux ratios because the way in which DM haloes are configured around the lens and along the line of sight is not explicitly parametrized by the model. Thus, inferring the properties of the halo mass function can only be done in a statistical manner, as we are not directly counting the number of DM haloes that give rise to the flux ratios, it is prudent to calculate what a MixDM signal, compared to WDM, might look like. The signal of the difference between WDM and MixDM would be a different distribution in the predictions of the flux ratios.

In Fig. 2, we see an example 2D histogram of flux ratios for CDM, WDM, and MixDM. The two dimensions in these figures are the flux ratios of the different images of a quadruply lensed system. This distribution is over the different realizations of DM subhaloes and line-of-sight haloes. The histograms in Fig. 2 represent the distribution over possible observed flux ratios for CDM, WDM, and MixDM. The statistical signal that has the potential to differentiate the models is the scatter in the models’ predictions, rather than the mean. The mean of the flux ratio anomaly method for all three models is similar, however, the distributions differ. CDM has the largest variance in the predictions of the flux ratios, followed by MixDM and then WDM, which follows simply from the fact CDM predicts the largest number of DM subhaloes, followed by MixDM and then WDM.

Further, we compress the full 3D information of flux ratios into a summary statistic that characterizes how different the observed flux ratios are from the flux ratios predicted by the smooth main lens. In particular, we compute these likelihoods by simulating the Z-statistic for a sampling of the different realizations of the distribution of line of sight and subhaloes.

The Z-statistic is defined as follows:

$$Z(f_i) = \sum_i (f_i - f_{\text{ref},i})^2, \quad (3)$$

where f_i are the flux ratios for the full model with the additional DM line-of-sight haloes and subhaloes, and $f_{\text{ref},i}$ is the reference image flux ratios that correspond to the predicted flux ratios from the macromodel of the main deflector lens when there are no additional DM line-of-sight haloes or subhaloes. The sum is over each of the images. We assume a fixed model of the main deflector and only

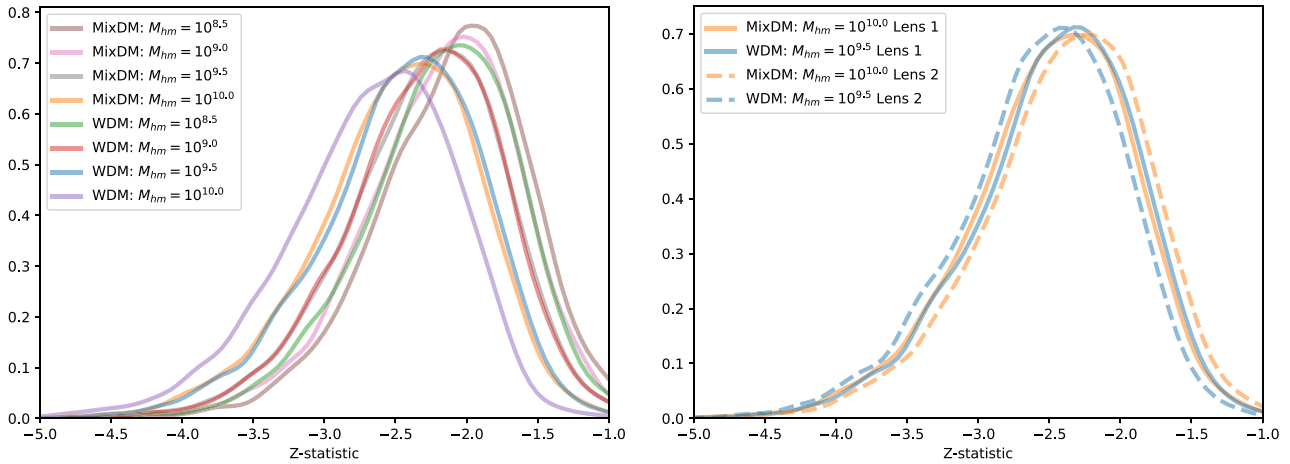


Figure 3. On the left, we show likelihoods of the Z-statistic for various half-mode masses for the WDM and MixDM cases for our first mock lens. Some of these distributions are identical, which would mean, no matter how many observations drawn from the distribution, they should be indistinguishable. On the right, we show likelihoods for $M_{hm} = 10^{10} M_{\odot}$ for the MixDM model and $M_{hm} = 10^{9.5} M_{\odot}$ for the WDM model, which overlap for the first lens, and likelihoods for the same parameters and models for the second lens, which do not overlap. Thus, if we combine information from different lenses with different lens configurations, we will be able to break these degeneracies.

allow for the realization of the DM substructure to vary. Similarly, for this initial test, we do not account for any statistical noise from the measurement of the fluxes of these quadruply lensed systems. Such noise would broaden these distributions in the same way between different models. This is an idealistic case but a useful one for demonstrating how WDM and MixDM are statistically different. We do this for different half-mode masses in the range for both the WDM and MixDM models.

In Fig. 3, we show the likelihood of the Z-statistic. We see that some of these likelihoods for WDM and MixDM are indistinguishable. For instance, the likelihood for the MixDM model with $M_{hm} = 10^{10} M_{\odot}$ and WDM model with $M_{hm} = 10^{9.5} M_{\odot}$ lie on top of each other.

This would imply that the two models, for these parameters, should be indistinguishable, no matter how many lenses are observed, and further, that even if DM was a mixture of warm and cold components, the corresponding suppression in the halo mass function could be interpreted as coming from a WDM model. However, these distributions were calculated for just a single lens configuration of the gravitational lens. The range of halo masses that flux ratios are sensitive to will generally depend on the configuration of the lensed images in addition to the size of the source.

To this end, we additionally test if the degeneracy between WDM and MixDM is the same between different lens configurations. Thus, we perform the same calculation for a different mock lens configuration. In Fig. 4, we show the two example lenses we use to make this point. We take the same WDM parameters ($M_{hm} = 10^{9.5} M_{\odot}$) and MixDM parameters ($M_{hm} = 10^{10} M_{\odot}$) that overlap in the first lens and calculate the distribution of their Z-statistics for the second lens. We find that the likelihoods are different for our second lens configuration; the distributions shift in different directions for the second lens. Thus, we find that a set of different lenses would at least weakly break any degeneracy between WDM and MixDM.

5 RESULTS

Now that we have demonstrated that observing lenses with multiple, different configurations of main deflectors can break degeneracies between WDM and MixDM, we want to be concrete about how

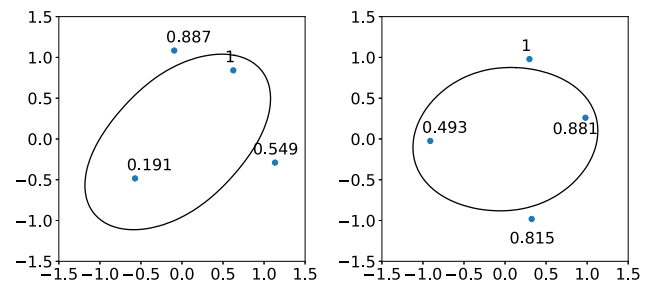


Figure 4. Configurations of the two lenses (lens 1 left, lens 2 right) in question and labelled by the flux ratios for each image. The critical curves are also displayed.

many lenses are needed to differentiate between CDM, WDM, and MixDM.

In order to do this calculation, we first create a set of flux ratio data sets from the MixDM model. That is, we create a set of mock lens configurations and populate these lenses with additional DM haloes generated statistically from the MixDM model. Specifically, we choose $\log_{10}(M_{hm}/M_{\odot}) = 8.5$, $\Sigma_{\text{sub}} = 0.05 \text{ kpc}^{-2}$, and $f = 0.5$. The flux ratios from these mock gravitational lens systems are our mock data sets.

The predictions of our strong lens modelling depend on not only the parameters of the lens and DM parameters, but also the specific configuration of DM subhaloes and line-of-sight haloes around the lens. This configuration is not parametrized but is implemented as a stochastic process. Because the forward modelling involves a stochastic process, standard statistical inference techniques, such as Markov chain Monte Carlo (MCMC) or nested sampling, cannot be used. Thus, we use approximate Bayesian computation (ABC) selection to approximate a posterior (Akeret et al. 2015; Birrer, Amara & Refregier 2017; Hahn et al. 2017). This method was used to constraint DM models including WDM, SIDM in previous works including Gilman et al. (2017, 2018, 2019, 2020b, 2021, 2022). ABC works by calculating a summary statistic (S) for how well the forward modelled flux ratios (f_i) match the data ($f_{\text{data},i}$). Specifically,

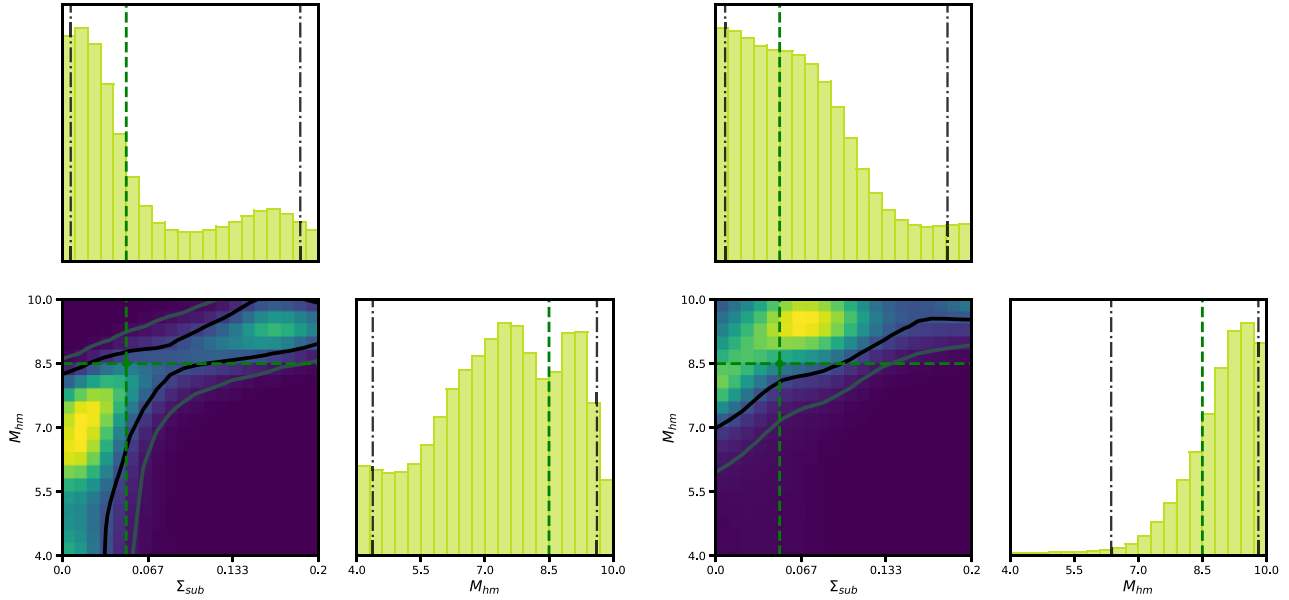


Figure 5. Posteriors for the half-mode mass and normalization of the subhalo mass function for 40 mock lenses for the WDM case (left) and for the MixDM case (right). The green line denotes the true parameters of the MixDM model that was used to generate the data.

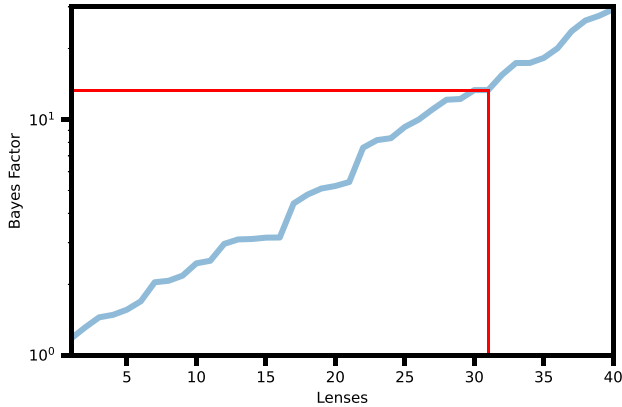


Figure 6. Cumulative Bayes factor between the MixDM and WDM models as a function of number of lenses. This surpasses the Jeffreys scale threshold for a ‘strong’ preference at 25 lenses, and at 40 lenses, prefers the MixDM model by a factor of 30:1. The red line corresponds to the forecasted statistical preference for the 31 lenses we will observe with upcoming *JWST* observations.

we choose an unweighted χ^2 statistic

$$S^2 = \sum_i (f_i - f_{\text{data},i})^2. \quad (4)$$

We use this S -statistic for inferring strong lensing parameters, rather than the Z -statistic, to follow previous studies such as Gilman et al. (2019, 2020b), where it has been extensively tested on simulated data and shown to robustly recover input model parameters. The ABC method then selects samples on the condition that the S -statistic is less than some threshold. We choose $S < 0.05$, which roughly corresponds to a < 3 per cent precision on individual flux ratios. We checked convergence by generating samples until the posterior stopped changing with increasing number of accepted samples. We checked that the threshold does not shift the posterior, just the contours become less noisy. We sample the prior uniformly in the range $\log_{10}(M_{\text{hm}}/M_{\odot}) \in \{4, 10\}$ and $\Sigma_{\text{sub}} \in \{0.0, 0.2\} \text{ kpc}^{-2}$. The

S -statistic for each of these prior samples are calculated and if the S -statistic for a given sample is less than our threshold criteria of $S < 0.05$, it is selected. This set of selected samples parameters compose the set of parameters that can provide a reasonable fit to the data and approximate parameter samples drawn from the posterior. In order to combine these approximate posteriors for each lens into a joint posterior, we then calculate a kernel density estimate for the set of selected samples. We calculate a joint posterior for the different lenses by simply multiplying the individual kernel density estimates.

Fig. 5 shows the results of these calculations, where we show the 1σ and 2σ contours of the joint posteriors for our 40 mock lenses. The simple rule of thumb to interpret these posterior plots is that the bottom right corner, with parameters $\Sigma_{\text{sub}} = 0.2 \text{ kpc}^{-2}$ and $\log_{10}M_{\text{hm}} = 4.0$ is the region with the most amount of structure, and the opposite upper left corner, with $\Sigma_{\text{sub}} = 0.0 \text{ kpc}^{-2}$ and $\log_{10}M_{\text{hm}} = 10.0$ is the region with the least amount of structure. The true value for the parameters, as indicated by the green lines, was a case with an intermediate amount of structure, from the MixDM case. The left-hand panel shows the results for the WDM case and the right-hand panel shows the case for the MixDM case. For a fixed fraction of CDM ($f = 0.5$), the MixDM model is necessarily less flexible than the WDM and predicts a narrower range of observables over its parameter space. For instance, in the MixDM case, the suppression in structure relative to CDM comes to a minimum value of the square of the CDM fraction (f^2) for small halo masses. This difference in the range of predictions for the two models is the explanation for the differences in the posteriors of the two models and what parameters they do and do not rule out. To explain, for the bottom right corner of parameter space, both models should have a large amount of structure that is observably indistinguishable, but the opposite, upper left corner for MixDM would predict categorically more structure than the WDM case. Since the true parameters correspond to roughly an intermediate amount of structure and the least amount of structure the MixDM can predict is an intermediate amount, the MixDM case cannot rule out the upper left corner. In the WDM case, the upper left corner corresponds to very little amount of structure which the

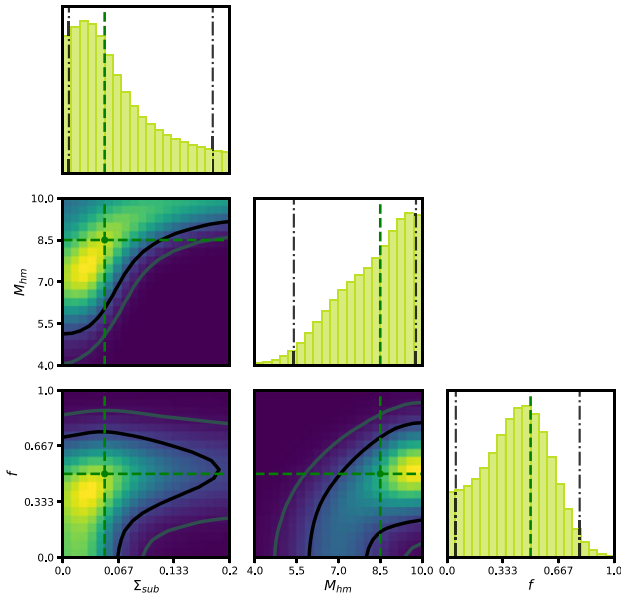


Figure 7. Posterior for the case where the CDM fraction f is varied alongside the half-mode mass M_{hm} and the normalization of the subhalo mass function Σ_{sub} .

data can rule out. Thus, the contours are less well constrained in the MixDM case than in the WDM case.

5.1 Bayesian evidences

The Bayesian evidence can also be approximated with the ABC method by simply calculating the frequency of a model satisfying the ABC criteria. Thus, we can calculate a Bayes factor for a single lens by calculating how more frequently will samples from one model satisfy the ABC criteria than another. We then calculate the Bayes factor for the set of lenses by multiplying the Bayes factors for the individual lenses. The result of this calculation is shown in Fig. 6, where we can see that it takes around 35 lenses to achieve a 20:1 preference for MixDM over WDM for our mock MixDM and at 40 lenses, the preference is at a level of 30:1. This relationship is linear in the log of the Bayes factor and so can be approximately extrapolated to a large number of lenses as would be expected from next-generation surveys.

5.2 Varying f

These previous results for the MixDM model were calculated with a fixed fraction of CDM ($f = 0.5$) and now in Fig. 7 we calculate the posteriors for the full model case where the fraction of CDM, f , is allowed to vary and the true value is $f = 0.5$. Examining the marginalized posterior for f , we can see that the CDM regime $f = 1$ is more easily ruled out than the WDM regime $f = 0$. This is a result of the only weakly broken degeneracies between CDM fraction, f , and the half-mode mass M_{hm} .

6 CONCLUSIONS

In this paper, we have forecasted the potential for flux ratio anomalies in strong gravitational lensing to be sensitive to forms of suppression of the halo mass function beyond WDM. To concretely demonstrate this point, we calculate the lensing signal from a MixDM model.

Since the anomalous flux method for detecting DM from strong lenses is sensitive to not just one mass scale of the halo mass function, but averaged over a range, it will be difficult to distinguish between different scenarios in which the halo mass function would be suppressed by different DM physics. Specifically, with only one lens configuration, a MixDM model could be confused for a WDM with a different half-mode mass. With a data set composed of multiple different lens configurations, this degeneracy can be broken.

One important caveat is that, at present, we have implemented the concentrations for MixDM haloes using the WDM concentration–mass relation. Since the MixDM concentration–mass relation is expected to be different, this can be a useful tool for differentiating the WDM and MixDM models from each other using strong lens systems. Robustly calculating what the MixDM concentration–mass relation should be is left for future work.

Further, we find that, with 40 lenses, we can use the ABC method to distinguish between a MixDM model and a WDM with a confidence of 30:1 for the case when f is fixed to 0.5. Further, with an upcoming *JWST* programme (GO-2046) which will observe 31 lenses, a Bayes factor of 13:1 can be achieved, and thus, a MixDM model that is maximally different than CDM or WDM should be detectable, and more generally, such strong gravitational lens systems would have sensitivities to suppression in the halo mass function beyond just the WDM paradigm. This prospect is exciting since, given that we can constrain these rather complex MixDM models, we might also be able to constrain other composite DM models or constrain features in the small-scale matter distribution.

ACKNOWLEDGEMENTS

We would like to acknowledge all of the academic workers in the University of California system who have been striking to improve working and living conditions. This research was conducted using [MERCED cluster (NSF-MRI, #1429783)/Pinnacles (NSF-MRI, #2019144)/Science DMZ (NSF-CC* #1659210)] at the Cyberinfrastructure and Research Technologies (CIRT) at University of California, Merced. TT and AMN acknowledge support by NSF through grants AST-2205100 ‘Collaborative Research: Measuring the physical properties of DM with strong gravitational lensing’, AST-1836016 ‘Astrophysics enabled by Keck All Sky Precision Adaptive Optics’, and by the Gordon and Betty Moore Foundation through grant. Support for programme #2046 was provided by NASA through a grant from the Space Telescope Institute, which is operated by the Association of Universities for Research in Astronomy, Inc., under NASA contract NAS 5-03127.

DATA AVAILABILITY

The data used in this work are mocks generated by the authors with the software packages PYHALO and LENSTRONOMY, as described in the text.

REFERENCES

- Abazajian K. N., 2017, *Phys. Rep.*, 711, 1
- Abazajian K. N., Kusenko A., 2019, *Phys. Rev. D*, 100, 103513
- Abazajian K., Fuller G. M., Patel M., 2001, *Phys. Rev. D*, 64, 023501
- Abazajian K. N., Horiuchi S., Kaplinghat M., Keeley R. E., Macias O., 2020, *Phys. Rev. D*, 102, 043012
- Akeret J., Refregier A., Amara A., Seehars S., Hasner C., 2015, *JCAP*, 08, 043
- Amara A., Metcalf R. B., Cox T. J., Ostriker J. P., 2006, *MNRAS*, 367, 1367

- Anderhalden D., Diemand J., Bertone G., Macciò A. V., Schneider A., 2012, *JCAP*, 10, 047
- Andrade K. E., Minor Q., Nierenberg A., Kaplinghat M., 2019, *MNRAS*, 487, 1905
- Andrade K. E., Fuson J., Gad-Nasr S., Kong D., Minor Q., Roberts M. G., Kaplinghat M., 2021, *MNRAS*, 510, 54
- Angulo R. E., Hahn O., Ludlow A. D., Bonoli S., 2017, *MNRAS*, 471, 4687
- Benson A. J., 2012, *New Astron.*, 17, 175
- Birrer S., Amara A., 2018, *Phys. Dark Univ.*, 22, 189
- Birrer S., Amara A., Refregier A., 2017, *JCAP*, 05, 037
- Birrer S. et al., 2021, *J. Open Source Softw.*, 6, 3283
- Bond J. R., Szalay A. S., 1983, *ApJ*, 274, 443
- Bose S., Hellwing W. A., Frenk C. S., Jenkins A., Lovell M. R., Helly J. C., Li B., 2016, *MNRAS*, 455, 318
- Boyarsky A., Lesgourgues J., Ruchayskiy O., Viel M., 2009, *JCAP*, 05, 012
- Chen J., Kravtsov A. V., Keeton C. R., 2003, *ApJ*, 592, 24
- Colombi S., Dodelson S., Widrow L. M., 1996, *ApJ*, 458, 1
- Dalal N., Kochanek C. S., 2002, *ApJ*, 572, 25
- Despali G., Giocoli C., Angulo R. E., Tormen G., Sheth R. K., Baso G., Moscardini L., 2016, *MNRAS*, 456, 2486
- Dodelson S., Widrow L. M., 1994, *Phys. Rev. Lett.*, 72, 17
- Dutton A. A., Macciò A. V., 2014, *MNRAS*, 441, 3359
- Enzi W. et al., 2021, *MNRAS*, 506, 5848
- Gaskins J. M., 2016, *Contemp. Phys.*, 57, 496
- Gilman D., Agnello A., Treu T., Keeton C. R., Nierenberg A. M., 2017, *MNRAS*, 467, 3970
- Gilman D., Birrer S., Treu T., Keeton C. R., Nierenberg A., 2018, *MNRAS*, 481, 819
- Gilman D., Birrer S., Treu T., Nierenberg A., Benson A., 2019, *MNRAS*, 487, 5721
- Gilman D., Birrer S., Nierenberg A., Treu T., Du X., Benson A., 2020a, *MNRAS*, 491, 6077
- Gilman D., Du X., Benson A., Birrer S., Nierenberg A., Treu T., 2020b, *MNRAS*, 492, L12
- Gilman D., Bovy J., Treu T., Nierenberg A., Birrer S., Benson A., Sameie O., 2021, *MNRAS*, 507, 2432
- Gilman D., Zhong Y.-M., Bovy J., 2022, *Phys. Rev. D*, 107, 103008
- Green A. M., Hofmann S., Schwarz D. J., 2004, *MNRAS*, 353, L23
- Hahn C., Vakili M., Walsh K., Hearin A. P., Hogg D. W., Campbell D., 2017, *MNRAS*, 469, 2791
- Hsueh J.-W., Enzi W., Vegetti S., Auger M. W., Fassnacht C. D., Despali G., Koopmans L. V. E., McKean J. P., 2020, *MNRAS*, 492, 3047
- Kahlhoefer F., 2017, *Int. J. Mod. Phys. A*, 32, 1730006
- Kamada A., Inoue K. T., Takahashi T., 2016, *Phys. Rev. D*, 94, 023522
- Kim S. Y., Peter A. H. G., 2021, preprint (arXiv:2106.09050)
- Kim S. Y., Peter A. H. G., Hargis J. R., 2018, *Phys. Rev. Lett.*, 121, 211302
- Kusenko A., 2009, *Phys. Rep.*, 481, 1
- Laroche A., Gilman D., Li X., Bovy J., Du X., 2022, *MNRAS*, 517, 1867
- Lesgourgues J., 2011, preprint (arXiv:1104.2932)
- Mao S., Schneider P., 1998, *MNRAS*, 295, 587
- Metcalf R. B., 2005, *ApJ*, 629, 673
- Metcalf R. B., Madau P., 2001, *ApJ*, 563, 9
- Minezaki T., Chiba M., Kashikawa N., Inoue K. T., Kataza H., 2009, *ApJ*, 697, 610
- Minor Q., Kaplinghat M., Chan T. H., Simon E., 2021a, *MNRAS*, 507, 1202
- Minor Q., Gad-Nasr S., Kaplinghat M., Vegetti S., 2021b, *MNRAS*, 507, 1662
- Miranda M., Maccio A. V., 2007, *MNRAS*, 382, 1225
- Moustakas L. A., Metcalf R. B., 2003, *MNRAS*, 339, 607
- Nadler E. O., Birrer S., Gilman D., Wechsler R. H., Du X., Benson A., Nierenberg A. M., Treu T., 2021, *ApJ*, 917, 7
- Niemeyer J. C., 2020, *Prog. Part. Nucl. Phys.*, 113, 103787
- Nierenberg A. M., Treu T., Menci N., Lu Y., Torrey P., Vogelsberger M., 2016, *MNRAS*, 462, 4473
- Nierenberg A. M. et al., 2020, *MNRAS*, 492, 5314
- Parimbelli G., Scelfo G., Giri S. K., Schneider A., Archidiacono M., Camera S., Viel M., 2021, *JCAP*, 12, 044
- Patwardhan A. V., Fuller G. M., Kishimoto C. T., Kusenko A., 2015, *Phys. Rev. D*, 92, 103509
- Planck Collaboration VI, 2020, *A&A*, 641, A6
- Robles V. H., Bullock J. S., Boylan-Kolchin M., 2019, *MNRAS*, 483, 289
- Schumann M., 2019, *J. Phys. G: Nucl. Part. Phys.*, 46, 103003
- Sheth R. K., Tormen G., 1999, *MNRAS*, 308, 119
- Shi X., Fuller G. M., 1999, *Phys. Rev. Lett.*, 82, 2832
- Vegetti S., Despali G., Lovell M. R., Enzi W., 2018, *MNRAS*, 481, 3661
- Viel M., Becker G. D., Bolton J. S., Haehnelt M. G., 2013, *Phys. Rev. D*, 88, 043502
- Vogel C. M., Abazajian K. N., 2022, preprint (arXiv:2210.10753)
- Vogt S. M. L., Marsh D. J. E., Laguë A., 2022, *Phys. Rev. D*, 107, 063526
- Wizinowich P. et al., 2022, in Schreiber L., Schmidt D., Vernet E., eds, *Proc. SPIE Conf. Ser. Vol. 12185, Adaptive Optics Systems VIII*. SPIE, Bellingham, p. 121850Q
- Wright S. et al., 2019, *Bull. Am. Astron. Soc.*, 51, 201
- Zelko I. A., Treu T., Abazajian K. N., Gilman D., Benson A. J., Birrer S., Nierenberg A. M., Kusenko A., 2022, *Phys. Rev. Lett.*, 129, 191301

This paper has been typeset from a $\text{\TeX}/\text{\LaTeX}$ file prepared by the author.